Microfabricated optofluidic ring resonator structures

Kee Scholten,[1,2] Xudong Fan,[1,3] and Edward. T. Zellers[1,2,4,5,a)]
[1]*Center for Wireless Integrated Microsensing and Systems, University of Michigan, Ann Arbor, Michigan 48109-2122, USA*
[2]*Applied Physics Program, University of Michigan, Ann Arbor, Michigan 48109-1040, USA*
[3]*Department of Biomedical Engineering, University of Michigan, Ann Arbor, Michigan 48109-2110, USA*
[4]*Department of Environmental Health Sciences, University of Michigan, Ann Arbor, Michigan 48109-2029, USA*
[5]*Department of Chemistry, University of Michigan, Ann Arbor, Michigan 48109-1055, USA*

(Received 23 August 2011; accepted 12 September 2011; published online 5 October 2011)

We describe the fabrication and preliminary optical characterization of rugged, Si-micromachined optofluidic ring resonator (μOFRR) structures consisting of thin-walled SiO_x cylinders with expanded midsections designed to enhance the three-dimensional confinement of whispering gallery modes (WGMs). These μOFRR structures were grown thermally at wafer scale on the interior of Si molds defined by deep-reactive-ion etching and pre-treated to reduce surface roughness. Devices 85-μm tall with 2-μm thick walls and inner diameters ranging from 50 to 200 μm supported pure-mode WGMs with Q-factors $>10^4$ near 985 nm. Advantages for eventual vapor detection in gas chromatographic microsystems are highlighted. © *2011 American Institute of Physics*. [doi:10.1063/1.3645629]

The development of optical ring resonators as transducers for (bio)chemical analysis has been a topic of intensive investigation recently.[1,2] The optofluidic ring resonator (OFRR) is unique among the members of this class of sensors because it naturally integrates sensing and fluidic functions.[3–6] The OFRR consists of a narrow capillary, the (thinned) wall of which supports whispering gallery modes (WGMs) that circulate along the circumference and interact with analytes passing through the capillary. Over the past five years, OFRRs have been shown capable of highly sensitive label-free biosensing[3,4,6–10] and vapor sensing.[11,12]

Most OFRRs reported to date have been fabricated by one of two methods. The first involves drawing a capillary pre-form under heat.[3–5] While devices made in this way have yielded resonances with high Q-factors (i.e., $>10^6$), they are not well-suited for integration in lab-on-a-chip microsystems; only a single device is made at a time, there can be considerable variation in diameter and wall thickness, and the OFRRs tend to be fragile. The second method employs a strain-induced self-rolling process applied to semiconductor multi-layers.[6,10,13–15] This method is amenable to mass production using standard microfabrication processes and yields devices with precise and reproducible diameters and wall thicknesses. But Q-factors reported for devices made in this way have generally been low (i.e., 10^2–10^3) and the diameters, which are just a few micrometers, pose significant challenges with respect to fluid throughput and interconnection with other components of integrated lab-on-chip microsystems in which we are interested.

In an attempt to address some of the shortcomings in existing OFRR designs, we have developed micromachined OFRR (μOFRR) structures suitable for ultimate integration in microanalytical systems such as the microscale gas chromatograph (μGC) prototypes on which we have reported recently.[16,17] Here, we describe the fabrication process and preliminary optical characterization of initial test structures as a prelude to evaluating their vapor sensitivity. Figure 1 shows a concept diagram of the basic configuration. Two designs were fabricated and tested: one with a straight-walled cylindrical shape and one with a cylinder having an expansion region at its midsection, inspired by OFRR "microbubbles."[18,19] An etched alignment channel was incorporated beside the cylinder to facilitate intimate contact with the tapered optical fiber used to couple the laser light source and photodetector to the μOFRR. Focusing on the design with the midsection expansion, we measured the Q-factor and the free spectral range (*FSR*) of several devices of different diameters.

Fabrication entailed first creating high-aspect-ratio cylindrical wells in a ⟨100⟩ Si wafer by deep reactive ion etching (DRIE) through a photoresist mask. Then, a conformal layer of C_4F_8 ~1 μm thick was deposited and subsequently removed from the floor of the etched wells using an extended anisotropic etch with SF_6. The masking layer of C_4F_8 remained on the sidewalls. In some devices, the floors of the wells were then etched isotropically by XeF_2 at 3 Torr to introduce an expansion in the cylinder. A second DRIE step continued the cylindrical fluidic path into the wafer with the original diameter. The initial photoresist mask and C_4F_8

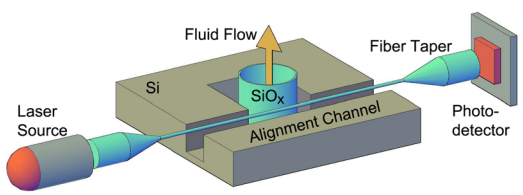

FIG. 1. (Color online) Diagram illustrating the basic structure and operation of the μOFRR.

a)Author to whom correspondence should be addressed. Electronic mail: ezellers@umich.edu.

layer were stripped in a bath of piranha etch. In the straight-walled devices, a second lithographic step defined a photoresist mask on the back side of the wafer, and a final DRIE step was used to etch completely through the wafer.

For devices fabricated with the midsection expansion, a 2-μm thick conformal SiO_x layer was grown by means of an extended wet oxidation at 1100 °C and then stripped in a bath of 1:1 HF and DI water. This step significantly reduced the surface roughness on the interior of the mold. Subsequently, a second 2-μm thick conformal SiO_x layer was grown and chemical/mechanical polishing was used to remove the SiO_x layer from the top surface of the wafer. Photoresist was then patterned to define a mask with openings for a 40-μm wide linear channel tangential to the cylinder, as well as annular trenches 90–240 μm wide (depending on cylinder diameter) surrounding the cylinder. These features were etched into the substrate with XeF_2 to a depth of 85 μm. Devices were then diced into chips 3×3 mm and cleaned to remove residual debris.

To test the devices, a fused-silica optical fiber was tapered down to less than 2 μm in diameter over a 6 mm length by heating with a H_2 flame and pulling the fiber under constant tension with a set of motors. The fiber was glued across a fixture with parallel support surfaces and the fixture was secured to an adjustable stage with a Vernier micrometer (Series 462, Newport, Irvine, CA) positioned above the μOFRR test chip. The fiber was lowered into the alignment channel in direct contact with the widest part of the μOFRR.

One end of the optical fiber was coupled to a 980 nm tunable diode-laser (Velocity 6320, New Focus, Irvine, CA) and the other to a large-area IR photoreceiver (2033, New Focus, Irvine, CA). Maintaining the laser output power between 2 and 6 mW, the wavelength was swept automatically from 980 to 990 nm at 0.25 nm/s and the detector voltage and wavelength were logged on a laptop computer running a custom LABVIEW data acquisition program (National Instruments, Austin, TX). Since the laser output and photoreceiver sensitivity varied independently with the wavelength, immediately following each measurement, the fiber was decoupled from the device and a baseline sweep was recorded. Three devices of each diameter were tested.

Discrete data from the photoreceiver were interpolated into a continuous function of laser wavelength and then divided by the baseline signal to extract the resonant waveform, which was subsequently normalized as a fraction of the maximum transmitted intensity. The full width at half maximum (FWHM) and center wavelength (i.e., the wavelength of minimum transmitted intensity) of each resonance were measured following curve fitting to a Lorentzian function using ORIGIN® software (OriginLab Corp., Northampton, MA).

The Q-factor (i.e., center wavelength/FWHM) was evaluated for each device at each resonant wavelength within the 980–990 nm window. The average Q-factor for a given device was determined from all of the measured resonances and then averaged for the three devices of a given diameter. The *FSR* was calculated as the average difference between the center wavelengths of successive resonances for devices of a given diameter. The resonant cavity length was taken as the circumference of the cylinder measured along the widest part of the structure by SEM. By assuming a pure circulating mode, the effective ring radius, r, was calculated for each device from each measured *FSR* as $r = \lambda^2/(2\pi n FSR)$, where the index of refraction, n, for the thermal SiO_x was taken as 1.46,[20] and λ is the center wavelength of resonance. The average r value was then calculated.

Figure 2 shows SEM images of one representative μOFRR of each design. The μOFRR chips were easily manipulated, transported, and tested without breakage. The straight-walled cylindrical structures (Figure 2(a)) were made first and served to demonstrate the feasibility of the fabrication process; however, tests of several devices failed to yield any resonances. We speculated that optical modes were propagating vertically from the point of contact and dissipating into the Si frame. So, a second set of devices was fabricated with midsection expansions, on the basis of previous reports suggesting that such contours can provide effective confinement of optical resonances.[21,22] These devices similarly failed to yield measurable resonances. Since SEM images revealed significant interior surface roughness and characteristic etch damage, our attention was drawn to this feature as a possible cause of device failure, and a third set of devices having midsection expansions was fabricated with an extra oxidation step added to smooth the interior surface prior to final growth of the μOFRR structures. These devices produced sharp resonances and were amenable to further characterization.

The average Q-factor among all of the devices tested was 12 600, corresponding to a *FWHM* of 74 pm for a resonance centered at 985 nm. For devices with inlet diameters of 50, 100, 150, and 200 μm (midsection diameters of 73, 131, 184, and 239 μm, respectively), the average Q-factors were 9300, 12 700, 15 000, and 13 500, respectively, which are apparently limited by the residual surface roughness incurred during the microfabrication. Relative standard deviations ranged from 17% to 34% indicating fairly good

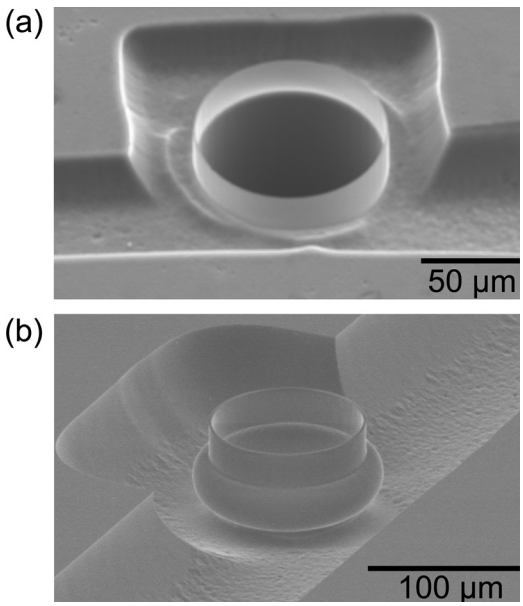

FIG. 2. SEM images of μOFRRs with embedded fiber-optic alignment channel: (a) 100-μm diameter straight-wall μOFRR; (b) 100-μm diameter μOFRR with mode confinement feature.

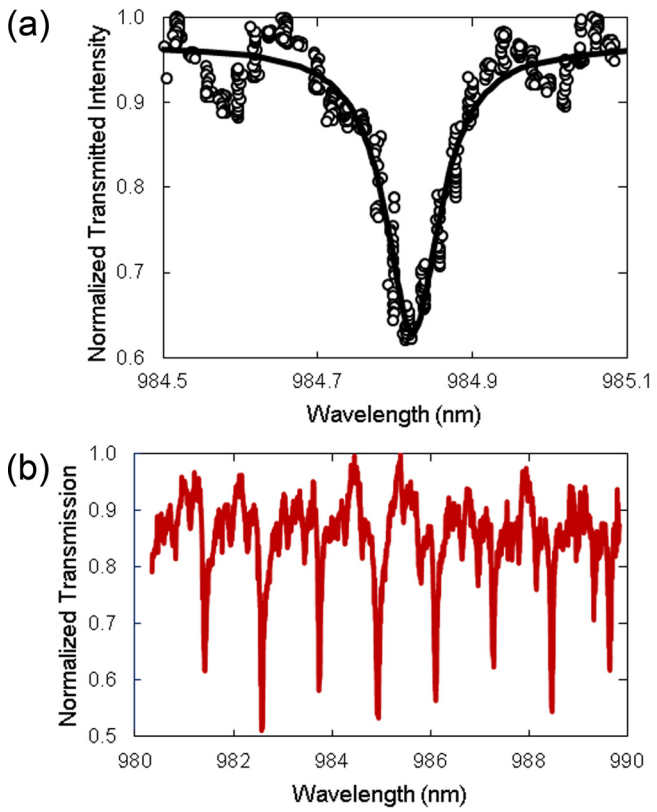

FIG. 3. (Color online) (a) Normalized WGM resonance centered at 984.83 nm generated in a 200-μm diameter μOFRR with midsection expansion (239 μm). Smooth curve represents the fit of the data to a Lorentzian function; (b) normalized transmission across a fiber waveguide coupled to a 150-μm diameter μOFRR during a 10 nm wavelength sweep of the laser source.

reproducibility. While the Q-factors observed here are lower than those of drawn-capillary OFRRs,[23] they are comparable to those of planar ring-resonators used as sensors of biomolecules[24] and volatile organic compounds.[25] (Note that another attribute of this μOFRR design is its use of SiO_x as the resonator material, which affords chemical inertness and low transmission loss over a wide range of wavelengths. SiO_x is not suitable for planar resonator designs because of strong coupling to the Si substrate.)

FSR values derived from the spacing of the resonances (e.g., Fig. 3(b)) ranged from 0.87 to 2.76 nm for the largest and smallest devices, respectively. The radii (cavity lengths) calculated on the basis of these measured *FSR* values differed by $<2\%$ from those determined by SEM measurements of the device dimensions, indicating that pure circulating WGMs are being confined within the midsection expansion regions of the devices.

In summary, we have demonstrated a facile process for creating hollow, three-dimensional SiO_x μOFRR structures with Q-factors exceeding 10^4. Measurements of the *FSR* confirm the presence of circulating WGMs similar to those induced in planar ring resonator devices. Advantages of this design over current drawn-capillary OFRRs include greater dimensional precision and ruggedness, batch fabrication, smaller size, thinner walls, and integral fiber-probe alignment, all of which should facilitate the implementation of μOFRR-based detectors in μGC and other lab-on-a-chip platforms. On-going work is focused on further reducing interior surface roughness, integrating micromachined fluidic interconnects with devices having completed fluidic channels, and testing vapor response characteristics with various sorptive interfacial films.

The authors express their heartfelt appreciation to Y. Sun, H. Li, G. Bahl, J. Zehnpfennig, and M. Tomes for technical assistance and helpful discussions. This work was supported by the Department of Homeland Security, Science and Technology Directorate, Cooperative Agreement 06-G-024. Additional support for K.S. was provided by the National Institutes of Health, Microfluidics in Biomedical Sciences Training Program, under Grant No. 2T32EB005582-06. Devices were fabricated in the Lurie Nanofabrication Facility, a member of the National Nanotechnology Infrastructure Network, which is supported by the National Science Foundation.

[1]F. Vollmer and S. Arnold, Nat. Methods **5**, 591 (2008).
[2]Y. Sun and X. Fan, Anal. Bioanal. Chem. **399**, 205 (2011).
[3]I. M. White, H. Oveys, and X. Fan, Opt. Lett. **31**, 1319 (2006).
[4]V. Zamora, A. Diez, M. V. Andres, and B. Gimeno, Opt. Express **15**, 12011 (2007).
[5]M. Sumetsky, Y. Dulashko, and R. S. Windeler, Opt. Lett. **35**, 898 (2010).
[6]A. Bernardi, S. Kiravittaya, A. Rastelli, R. Songmuang, D. J. Thurmer, M. Benyoucef, and O. G. Schmidt, Appl. Phys. Lett. **93**, 094106 (2008).
[7]H. Zhu, P. S. Dale, C. W. Caldwell, and X. Fan, Anal. Chem. **81**, 9858 (2009).
[8]X. Fan, S. I. Shopova, H. Zhu, and P. Zhang, Appl. Phys. Lett. **90**, 221101 (2007).
[9]X. Fan, Y. Sun, S. I. Shopova, C. S. Wu, and S. Arnold, Proc. Natl. Acad. Sci. U.S.A. **107**, 16039 (2010).
[10]G. S. Huang, V. A. B. Quinones, F. Ding, S. Kiravittaya, Y. F. Mei, and O. G. Schmidt, ACS Nano **4**, 3123 (2010).
[11]S. I. Shopova, I. M. White, Y. Sun, H. Zhu, X. Fan, G. Frye-Mason, A. Thompson, and S.-J. Ja, Anal. Chem. **80**, 2232 (2008).
[12]Y. Sun, J. Liu, D. J. Howard, X. Fan, G. Frye-Mason, S.-J. Ja, and A. K. Thompson, Analyst **135**, 165 (2010).
[13]S. Vicknesh, F. Li, and Z. Mi, Appl. Phys. Lett. **94**, 081101 (2009).
[14]I. Chun, K. Bassett, A. Challa, and X. Li, Appl. Phys. Lett. **96**, 251106 (2010).
[15]E. J. Smith, S. Schulze, S. Kiravittaya, Y. Mei, S. Sanchez, and O. G. Schmidt, "Lab-in-a-Tube: Detection of Individual Mouse Cells for Analysis in Flexible Split-Wall Microtube Resonator Sensors," Nano Lett. DOI: 10.1021/nl1036148
[16]C. J. Lu, W. H. Steinecker, W. C. Tian, M. C. Oborny, J. M. Nichols, M. Agah, J. A. Potkay, H. K. L. Chan, J. Driscoll, R. D. Sacks, K. D. Wise, S. W. Pang, and E. T. Zellers, Lab Chip **5**, 1123 (2005).
[17]S. K. Kim, H. Chang, and E. T. Zellers, Anal. Chem. **83**(18), 7198 (2011)
[18]M. Sumetsky, Y. Dulashko, and R. S. Windeler, Opt. Lett. **35**, 898 (2010).
[19]H. Li, Y. Guo, Y. Sun, K. Reddy, and X. Fan, Opt. Express **18**, 25081 (2010).
[20]W. Haynes and D. Lide, *CRC Handbook of Chemistry and Physics* (Taylor & Francis Group, Gaithersburg, MD, 2010).
[21]M. Sumetsky, Opt. Lett. **29**, 8 (2004).
[22]Y. Louyer, D. Meschede, and A. Rauschenbeutel, Phys. Rev. A **72**, 031801 (2005).
[23]Y. Sun, S. I. Shopova, G. Frye-Mason, and X. Fan, Opt. Lett. **33**, 788 (2008).
[24]A. Yalcin, K. C. Popat, J. C. Aldridge, T. A. Desai, J. Hryniewicz, N. Chbouki, B. E. Little, O. King, V. Van, S. Chu, D. Gill, M. Anthes-Washburn, and M. S. Unlu, IEEE J. Sel. Top. Quantum Electron. **12**, 148 (2006).
[25]N. A. Yebo, P. Lommens, Z. Hens, and R. Baets, Opt. Express **18**, 11859 (2010).